

# Multiobjective Test Problems with Complicated Pareto Fronts: Difficulties in Degeneracy

Hui Li

School of Mathematics and Statistics  
Xi'an Jiaotong University  
Xi'an, Shaanxi, China  
Email: lihui10@mail.xjtu.edu.cn

Qingfu Zhang

Department of Computer Science  
City University of Hong Kong  
Hongkong, China  
Email: qingfu.zhang@cityu.edu.hk

Jingda Deng

School of Mathematics and Statistics  
Xi'an Jiaotong University  
Xi'an, Shaanxi, China

**Abstract**—It is well-established that the shapes of Pareto-optimal fronts (POFs) can affect the performance of some multiobjective optimization methods. The most well-known characteristics on the shape of POFs are convexity and discontinuity. In this paper, we investigate the construction of multiobjective test problems with complicated POFs, of which its local parts could have mixed dimensionalities. For example, in the case of 3 objectives, some parts of POFs can be 1-D curves while others could be 2-D surfaces. We formulate eight test problems, called CPFT1-8, with such a feature. To study the difficulties of these test problems, we conducted some experiments with two state-of-the-art algorithms MOEA/D and NSGA-II, and analyzed their performances.

## I. INTRODUCTION

In the research community of evolutionary multiobjective optimization (EMO), the construction of test problems with various difficulties has motivated the birth of many classical EMO algorithms[1]. The well-known problem difficulties include the shapes of POFs (eg. convex, nonconvex, and disconnected), multimodality (i.e., many local pareto fronts) [2], [3], complicated Pareto-optimal sets (POSSs) (i.e., nonlinearity in variable space)[4], [5], [6], [7]. Among these difficulties, the shape of POFs has been studied over more than ten years. However, the POF shapes of many existing test problems are  $(m-1)$ -D manifold ( $m$  is the number of objective functions) in objective space according to Karush-Kuhn-Tucker condition [8]. Such a property is called regularity. Compared with classical multiobjective methods in mathematical programming, EMO algorithms, such as SPEA2[9], NSGA-II [10], MOEA/D [11], IBEA[12], are not sensitive to the convexity and nonconvexity of POFs.

In [13], a set of benchmark MOPs, called ZDT test problems, were studied and tested by several state-of-the-art EMO algorithms. Five out of six bi-objective ZDT problems have one-dimensional connected or disconnected POF (ZDT3) in the objective space. However, ZDT test problems can be easily solved by many recent EMO algorithms since their POSSs are linearly distributed in the decision space. To study the MOP with many objectives, a set of benchmark 3-objective MOPs were suggested in [14]. Among these test problems, the POF of DTLZ1 is a 3-D simplex while that of DTLZ2 is part of a sphere surface. The POFs of both test problems are two-dimensional manifold. However, some DTLZ test problems with degenerate POFs don't follow the regularity property. For example, the POFs of DTLZ5 and DTLZ6 are only a one-

dimensional curve with the dimensionality less than  $m-1$ . The degeneracy of POFs can cause difficulties for decomposition-based EMO algorithms, such as MOEA/D. The reason is that the optimal solutions of subproblems in MOEA/D can not approximate the whole POF well.

In this paper, we propose a two-step scheme based on coordinate transformation to design a set of test problems with complicated POFs with degeneracy, called CPFT test problems. Unlike the existing MOPs with degenerate POFs, our test problems could have both one-dimensional and two-dimensional local POFs at the same time. All test problems are designed on the basis of the toolkit for MOPs with complicated POSSs in [6], in which the objective function is the sum of a shape function and a distance function.

The rest of this paper is organized as follows. Section II introduces the construction toolkit for generating MOPs with degenerated POFs. A set of eight test problems are formulated and analyzed in Section III. In the following section, we experimentally compare the performance of two EMO algorithms, i.e., MOEA/D and NSGA-II on our new test problems. The final section concludes the paper.

## II. CONSTRUCTION TOOLKIT

In our earlier work [6], we have suggested the general framework for constructing test problems with complicated POSSs in decision space as follows:

$$f_i(x) = \alpha_i(x_{1:m-1}) + \beta_i(x_{1:m-1}, x_{m:n}) \quad (1)$$

where  $x_{1:m-1} = (x_1, \dots, x_{m-1})^T$ ,  $x_{m:n} = (x_m, \dots, x_n)^T$  are two subvectors of  $x = (x_1, \dots, x_n)^T$ . The objective function  $f_i(x)$ ,  $i = 1, \dots, m$  is the sum of shape function  $\alpha_i(x_{1:m-1})$  and nonnegative distance function  $\beta_i(x_{1:m-1}, x_{m:n})$ . Here,  $\beta_i(x_{1:m-1}, x_{m:n}) = 0$  only if  $x_{m:n}$  is the function of  $x_{1:m-1}$ , i.e.,  $x_{m:n} = g(x_{1:m-1})$ .

Based on above framework, we propose a toolkit for constructing three-objective test problems with degenerate POFs, which could have mixed dimensionality. To achieve this goal, we suggest a two-step scheme to design special 3-D surfaces, of which the nondominated points could belong to either 1-D curves or 2-D surfaces, or both. First, a 2-D curve is generated in a  $v$ - $o$ - $u$  plane shown in Fig 1, and is rotated by a certain angle plotted in Fig 2. Then, we move the origin of  $v$ - $o$ - $u$  plane along a 3-D curve visualized in Fig 3. The shape function

$\alpha_i, i = 1, 2, 3$  has the form:

$$\begin{bmatrix} \alpha_1(x_1, x_2) \\ \alpha_2(x_1, x_2) \\ \alpha_3(x_1, x_2) \end{bmatrix} = \begin{bmatrix} O_x(x_1) \\ O_y(x_1) \\ O_z(x_1) \end{bmatrix} + A \begin{bmatrix} v(x_2) \\ u(x_1, x_2) \\ 0 \end{bmatrix} \quad (2)$$

with

- The feasible region of decision variables is  $\Omega = [0, 1]^2 \times [-2, 2]^{n-2}$ . Intermediate variables  $u$  and  $v$  are the functions of  $x_1$  and  $x_2$ . The relationship between  $u$  and  $v$  determines the shape of POFs;
- $(O_x, O_y, O_z)$  represents the origin of curve ( $v = v(x_2), u = u(x_1, x_2)$ ). It moves in the 3-D space as the parameter  $x_1$  changes;
- The matrix  $A$  for rotating coordinate system is

$$A = \begin{bmatrix} \sin \frac{\pi}{4} & \cos \frac{\pi}{4} & 0 \\ -\cos \frac{\pi}{4} & \sin \frac{\pi}{4} & 0 \\ 0 & 0 & 0 \end{bmatrix};$$

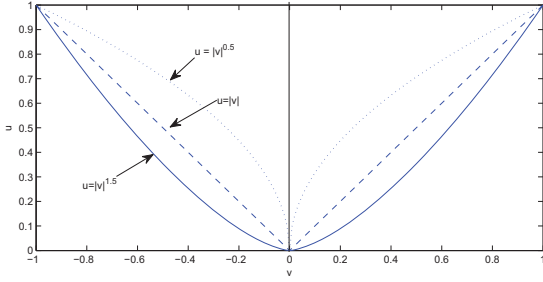


Fig. 1. POF curves in  $v$ - $o$ - $u$  coordinate system

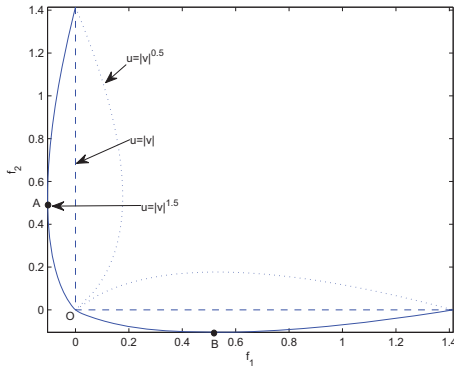


Fig. 2. POF curves in  $f_1$ - $o$ - $f_2$  coordinate system after rotating 45 degrees

The distance function  $\beta_j, j = 1, 2, 3$  can be formulated as:

$$\beta_j(x_{1:2}, x_{3:n}) = \sum_{i \in I_j} (x_i - x_2 \sin(2x_1 \pi))^2$$

where  $I_j = \{i | \text{mod}(i, 3) = j - 1, i \in \{3, 4, \dots, n\}\}, j = 1, 2, 3$ . It controls the shape of POSS, in which the relationship between  $x_i \in [-2, 2]$  and  $x_{1:2}$  of nondominated solutions can be stated as:

$$\bar{\Omega} = \{x \in \Omega | x_i = x_2 \sin(2\pi x_1), i = 3, \dots, n\}. \quad (3)$$

In the following, we give an example to explain how to generate an instance in detail. First, the curve in  $v$ - $o$ - $u$  coordinate system is defined by

$$u(x_1, x_2) = |v(x_2)|^{w(x_1)}$$

where  $v(x_2) = 2x_2 - 1$ , and  $w(x_1) = x_1 + 0.5$ . Therefore, the range of  $v$  is  $[-1, 1]$ , and that of  $w$  is  $[0.5, 1.5]$ . Fig 1 plots three curves with  $x_1 = 0, 0.5, 1$  resulting in  $w = 0.5, 1.0, 1.5$ , and Fig 2 shows the corresponding curves after being rotated by the angle  $\pi/4$  along a clockwise direction. It can be seen that the origin  $O$  is the only nondominated point in the curve when  $w(x_1) \leq 1$ . In contrast, a part of the curve, i.e., arc  $\widehat{AOB}$  in Fig 2, are nondominated when  $w(x_1) > 1$ . Then, the 3-D curve of moving the origin of  $v$ - $o$ - $u$  coordinate system is given by:

$$(O_x, O_y, O_z) = (x_1, x_1, -(2x_1 - 1)^3)$$

The corresponding curve is shown in Fig 3.

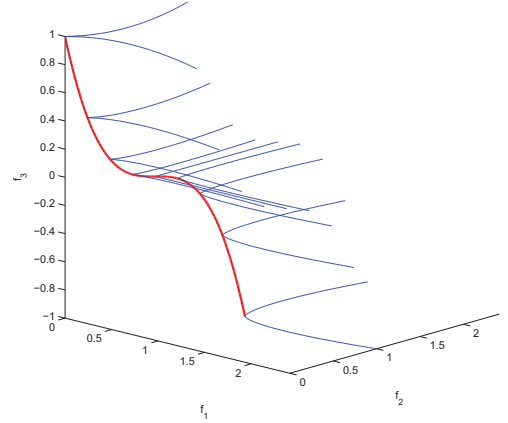


Fig. 3. A family of 2-D curves obtained with origins  $(x_1, x_1, -(2x_1 - 1)^3)$  where  $x$  changes from 0 to 1.

Using above configurations, we obtain the test instance CPFT3 suggested in this paper. All Pareto-optimal solutions are located along the following surface (visualized in Fig 6):

$$\begin{bmatrix} \alpha_1(x_{1:2}) \\ \alpha_2(x_{1:2}) \\ \alpha_3(x_{1:2}) \end{bmatrix} = \begin{bmatrix} x_1 + \cos \frac{\pi}{4} (2x_2 - 1) + \sin \frac{\pi}{4} \gamma(x_{1:2}) \\ x_1 - \sin \frac{\pi}{4} (2x_2 - 1) + \cos \frac{\pi}{4} \gamma(x_{1:2}) \\ -(2x_1 - 1)^3 \end{bmatrix} \quad (4)$$

where  $\gamma(x_{1:2}) = |2x_2 - 1|^{x_1 + 0.5}$ .

### III. THREE-OBJECTIVE TEST INSTANCES WITH DEGENERATED POFs

In this section, we suggested eight test instances with complicated POF - CPFT1-CPFT8 using above toolkit. Six of them have degenerate POFs.

- Test Instance 1 - CPFT1:

$$\begin{bmatrix} \alpha_1(x_{1:2}) \\ \alpha_2(x_{1:2}) \\ \alpha_3(x_{1:2}) \end{bmatrix} = \begin{bmatrix} x_1 \\ x_1 + 0.2 \sin(4x_1 \pi) \\ -(2x_1 - 1)^3 \end{bmatrix} + A \begin{bmatrix} 2x_2 - 1 \\ \gamma(x_{1:2}) \\ 0 \end{bmatrix} \quad (5)$$

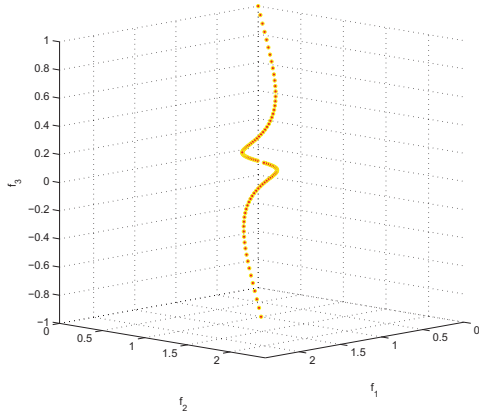


Fig. 4. The POFT1 in objective space

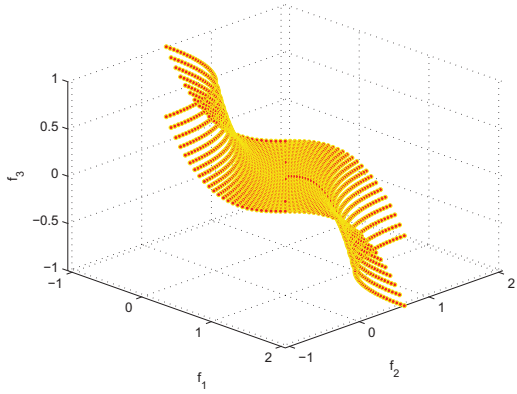


Fig. 5. The POFT2 in objective space

where

- $x = (x_1, \dots, x_n) \in \Omega = [0, 1]^n$ , and
- $\gamma(x_{1:2}) = |2x_2 - 1|^{0.5x_1+0.5}$ .

The POFT shape of CPFT1 is a 1-D curve in 3-D objective space shown in Fig. 4. It can be observed that the relationships among objectives are nonlinear. The resultant shape of its POFT is a complicated curve.

- Test Instance 2 - CPFT2:

$$\begin{bmatrix} \alpha_1(x_{1:2}) \\ \alpha_2(x_{1:2}) \\ \alpha_3(x_{1:2}) \end{bmatrix} = \begin{bmatrix} x_1 \\ x_1 \\ -(2x_1 - 1)^3 \end{bmatrix} + A \begin{bmatrix} 2x_2 - 1 \\ \gamma(x_{1:2}) \\ 0 \end{bmatrix} \quad (6)$$

where

- $x = (x_1, \dots, x_n) \in \Omega = [0, 1]^n$ , and
- $\gamma(x_{1:2}) = 0.5(2x_1 - 1)(2x_2 - 1)^2$

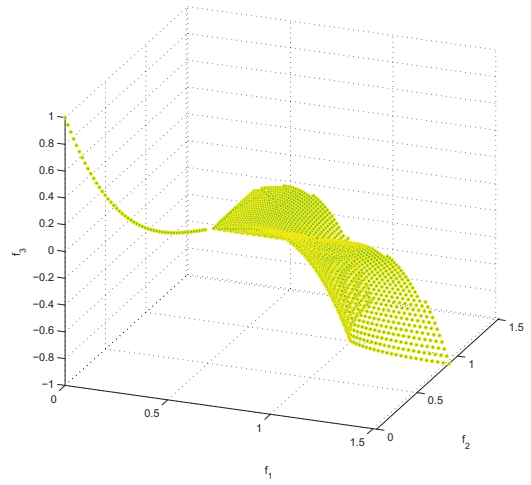


Fig. 6. The POFT3 in objective space

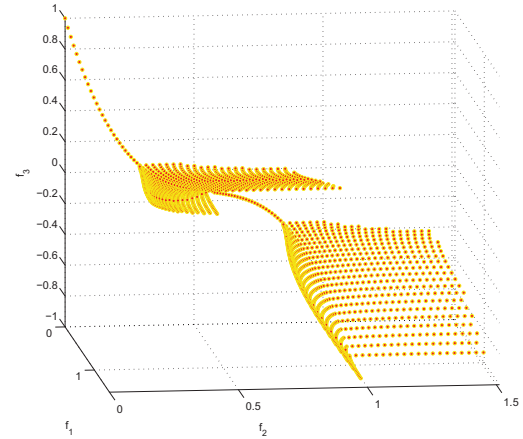


Fig. 7. The POFT4 in objective space

The POFT shape of CPFT2, shown in Fig. 5, is a part of 3-D surface, which is neither convex nor concave.

- Test Instance 3 - CPFT3:

$$\begin{bmatrix} \alpha_1(x_{1:2}) \\ \alpha_2(x_{1:2}) \\ \alpha_3(x_{1:2}) \end{bmatrix} = \begin{bmatrix} x_1 \\ x_1 \\ -(2x_1 - 1)^3 \end{bmatrix} + A \begin{bmatrix} 2x_2 - 1 \\ \gamma(x_{1:2}) \\ 0 \end{bmatrix} \quad (7)$$

where

- $x = (x_1, \dots, x_n) \in [0, 1]^n$  and
- $\gamma(x_{1:2}) = |2x_2 - 1|^{x_1+0.5}$ .

In this instance, the POFT consists of two parts plotted in Fig. 6. One of its parts is 1-D curve.

- Test Instance 4 - CPFT4:

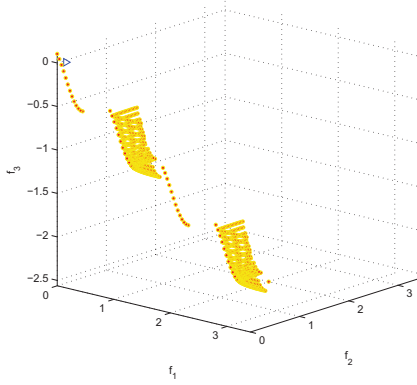


Fig. 8. The POFT of CPFT5 in objective space

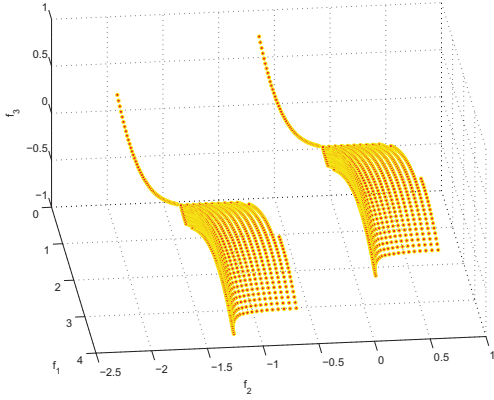


Fig. 9. The POFT of CPFT6 in objective space

$$\begin{bmatrix} \alpha_1(x_{1:2}) \\ \alpha_2(x_{1:2}) \\ \alpha_3(x_{1:2}) \end{bmatrix} = \begin{bmatrix} x_1 \\ x_1 \\ -(2x_1 - 1)^3 \end{bmatrix} + A \begin{bmatrix} 2x_2 - 1 \\ \gamma(x_{1:2}) \\ 0 \end{bmatrix} \quad (8)$$

where

- $x = (x_1, \dots, x_n) \in [0, 1]^n$
- $\gamma(x_{1:2}) = |2x_2 - 1|^{1.0-0.5 \sin(4x_1 \pi)}$ ,

In this instance, the POFT consists of four parts plotted in Fig. 7. Two are 1-D curves, and the other two parts are 2-D surfaces. Note that all four parts are connected.

- Test Instance 5 - CPFT5:

$$\begin{bmatrix} f_1(x) \\ f_2(x) \\ f_3(x) \end{bmatrix} = \begin{bmatrix} 2x_1 \\ 2x_1 \\ \gamma_1(x_{1:2}) \end{bmatrix} + A \begin{bmatrix} 2x_2 - 1 \\ \gamma_2(x_{1:2}) \\ 0 \end{bmatrix} \quad (9)$$

where

- $x = (x_1, \dots, x_n) \in [0, 1]^n$ , and

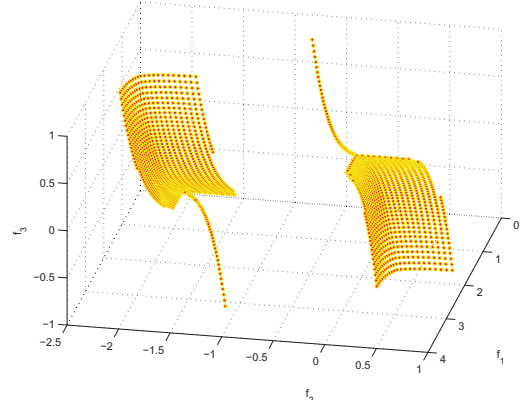


Fig. 10. The POFT of CPFT7 in objective space

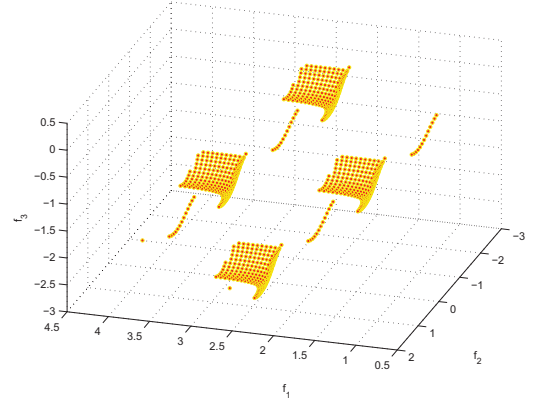


Fig. 11. The POFT of CPFT8 in objective space

- $\gamma_1(x_{1:2}) = 0.2 \cos(3\pi s(a, b, x_1)) - s(a, b, x_1)$  with  $s = a + 4bx_1$  ( $a = 6.217210009329 \times 10^{-2}$ ,  $b = 2/3$ ).
- $\gamma_2(x_{1:2}) = |2x_2 - 1|^{1.0-0.5 \sin(4x_1 \pi)}$

The POFT of this instance consists of four parts shown in Fig. 8. Two are 1-D curves, and the other two parts are 2-D surfaces. Unlike the POFT of CPFT4, all four parts are disconnected.

- Test Instance 6 - CPFT6:

$$\begin{bmatrix} f_1(x) \\ f_2(x) \\ f_3(x) \end{bmatrix} = \begin{bmatrix} x_1 \\ x_1 \\ -(2x_1 - 1)^3 \end{bmatrix} + A \begin{bmatrix} 2kx_2 \\ \gamma(x_{1:2}) \\ 0 \end{bmatrix} \quad (10)$$

where

- $x = (x_1, \dots, x_n) \in [0, 1]^n$
- $\gamma(x_{1:2}) = |2((kx_2) - \lfloor(kx_2)\rfloor) - 1|^{0.5+x_1}$ . Here,  $k$  is a positive integer number for controlling the number of parallel POFTs. In this work,  $k$  is set to 2.

The POFT of this instance has two parallel local POFTs with the same shape shown in Fig. 9.

- Test Instance 7 - CPFT7:

$$\begin{bmatrix} f_1(x) \\ f_2(x) \\ f_3(x) \end{bmatrix} = \begin{bmatrix} x_1 \\ x_1 \\ -(2x_1 - 1)^3 \end{bmatrix} + A \begin{bmatrix} 2kx_2 \\ \gamma(x_{1:2}) \\ 0 \end{bmatrix} \quad (11)$$

where

- $x = (x_1, \dots, x_n) \in [0, 1]^n$
- $\gamma(x_{1:2}) = |2((kx_2) - \lfloor(kx_2)\rfloor) - 1|^{p(k, x_1, x_2)}$
- $p(k, x_1, x_2)$  is defined as:

$$p(k, x_1, x_2) = \begin{cases} 0.5 + x_1 & \text{if } \text{mod}(\lfloor kx_2 \rfloor, 2) = 0 \\ 1.5 - x_1 & \text{otherwise} \end{cases}$$

The POF of this instance has two parallel local POFs plotted in Fig. 10, where the positions of 1-D manifolds and 2-D manifolds are inverse as  $x_1$  changes from 0 to 1.

- Test Instance 8 - CPFT8:

$$\begin{bmatrix} f_1(x) \\ f_2(x) \\ f_3(x) \end{bmatrix} = \begin{bmatrix} 2x_1 \\ 2x_1 \\ \gamma_1(x_{1:2}) \end{bmatrix} + A \begin{bmatrix} 2kx_2 \\ \gamma_2(x_{1:2}) \\ 0 \end{bmatrix} \quad (12)$$

where

- $x = (x_1, \dots, x_n) \in [0, 1]^n$ ;
- $\gamma_1(x_{1:2}) = 0.2 \cos(3\pi s(a, b, x_1)) - s(a, b, x_1)$  with  $s = a + 4bx_1$  and  $a = 6.217210009329 \times 10^{-2}$ ,  $b = 2/3$ ;
- $\gamma_2(x_{1:2}) = |2((kx_2) - \lfloor(kx_2)\rfloor) - 1|^{p(k, x_1, x_2)}$  with

$$p(k, x_1, x_2) = \begin{cases} 1 - 0.5 \sin(4x_1\pi) & \text{if } \text{mod}(\lfloor kx_2 \rfloor, 2) = 0 \\ 1 - 0.5 \sin(4(1 - x_1)\pi) & \text{otherwise} \end{cases}$$

Note that the integer  $k$  acts as the same role in CPFT7. The POF of this instance has parallel disconnected local POFs shown in Fig 11.

Note that the method introduced in this work can also be extended to construct the MOPs with many objectives. One of the simple way to do this is to combine the CPFT problems with some existing many-objective test problems. Due to the limitation on the pages, the details are not discussed in this work.

#### IV. COMPUTATIONAL EXPERIMENTS

In this section, we mainly compare the performance of two EMO algorithms, i.e., NSGA-II and MOEA/D, on the test instances introduced in the previous section.

#### A. Experimental settings

To check the difficulties of the test instances suggested in this paper, we consider two popular EMO algorithms (i.e., NSGA-II and MOEA/D) in our experiments. All eight instances CPFT1-CPFT8 have 3 objectives and 10 variables. The population size in both algorithms is set to 300. The total number of function evaluations is 50000 for all instances.

Since the recombination operators play very important role in the performance of EMO algorithms, we consider two versions of NSGA-II and MOEA/D with either simulated binary crossover (SBX) and differential evolution (DE) operators in comparison. Therefore, four algorithms, i.e., NSGA-II/SBX, NSGA-II/DE, MOEA/D-SBX, and MOEA/D-DE, are considered. The details of these algorithms can be referred to [7][10]. The scaling factor used in DE operator is set to 0.5 in both NSGA-II/DE and MOEA/D-DE. The distribution index used in SBX operator is 20. In all four algorithms, polynomial mutation with the distribution index equal to 20 is used for diversity.

To quantitatively measure the performance of MOEA/D and NSGA-II, we use the inverted generational distance (IGD) as the indicator in this work. It calculate the average Euclidean distances from the solutions in a reference set to the set of final solutions found by MOEA/D or NSGA-II. The good approximation of Pareto front both in convergence and in diversity will result in small IGD value.

#### B. Experimental results and discussions

In Table I, the mean and standard deviation of IGD values obtained by MOEA/D-DE, MOEA/D-SBX, NSGA-II/DE, and NSGA-II/SBX are provided. It is evident that MOEA/D-DE performed better than other three algorithms on all test instances in terms of IGD values. In two versions of MOEA/D, DE operator worked better than SBX operator. However, this is not the case in two versions of NSGA-II, where SBX operator is better than DE operator on most of test instances. In fact, the Pareto sets of all test instances are nonlinearly distributed in the variable space. The DE operator will produce more Pareto solutions only if the selected mating parents with similar structure in variable space are close to the Pareto front.

From the results in Table I, we can observe that NSGA-II/SBX performed better than NSGA-II/DE on most of the instances in terms of IGD metric. However, this observation is not consistent with some conclusions reported in the literatures that DE operator should in principle be better than SBX operator for MOPs with interacting variables. In fact, this is can be explained by the poor performance of NSGA-II in convergence. We should note that the DE operator is efficient only if the population is close to the Pareto front. In our experiments, we found that the populations of NSGA-II are still far from the POFs.

To compare the convergence speed of four algorithms, the evolution of IGD values on eight test instances in 20 runs are plotted in Figs. 12-15. It is clear that MOEA/D-DE performed much better than other three algorithms on all instances except CPFT5 and CPFT8 in convergence. On CPFT5 and CPFT8, MOEA/D-DE is slightly worse than NSGA-II/SBX. From these results, we can also note that the IGD values found by

TABLE I. THE MEAN AND STANDARD DEVIATION OF IGD VALUES FOUND BY MOEA/D AND NSGA-II

Instance	MOEA/D-DE	MOEA/D-SBX	NSGA-II/DE	NSGA-II/SBX
CPFT1	<b>0.0406173</b> (0.0056687)	0.2801804 (0.0710155)	0.2308281 (0.0340135)	0.1881514 (0.0330668)
CPFT2	<b>0.1202772</b> (0.0021441)	0.2988698 (0.0380437)	0.3615820 (0.0415087)	0.3678817 (0.0369457)
CPFT3	<b>0.0646472</b> (0.0020311)	0.1320251 (0.0172157)	0.1950159 (0.0490384)	0.1584895 (0.0277822)
CPFT4	<b>0.0607534</b> (0.0014359)	0.2030775 (0.0553320)	0.1890046 (0.0387380)	0.1153559 (0.0138797)
CPFT5	<b>0.1134535</b> (0.0050791)	0.3022815 (0.0717879)	0.1597766 (0.0277217)	0.1145035 (0.0171510)
CPFT6	<b>0.1089840</b> (0.0045082)	0.1975272 (0.0362393)	0.2157054 (0.0323819)	0.1686928 (0.0142450)
CPFT7	<b>0.0978083</b> (0.0030300)	0.3157848 (0.0432048)	0.2703440 (0.0627119)	0.1758781 (0.0260858)
CPFT8	<b>0.1414703</b> (0.0062645)	0.3903011 (0.0593595)	0.2712471 (0.0395323)	0.1554484 (0.0173572)

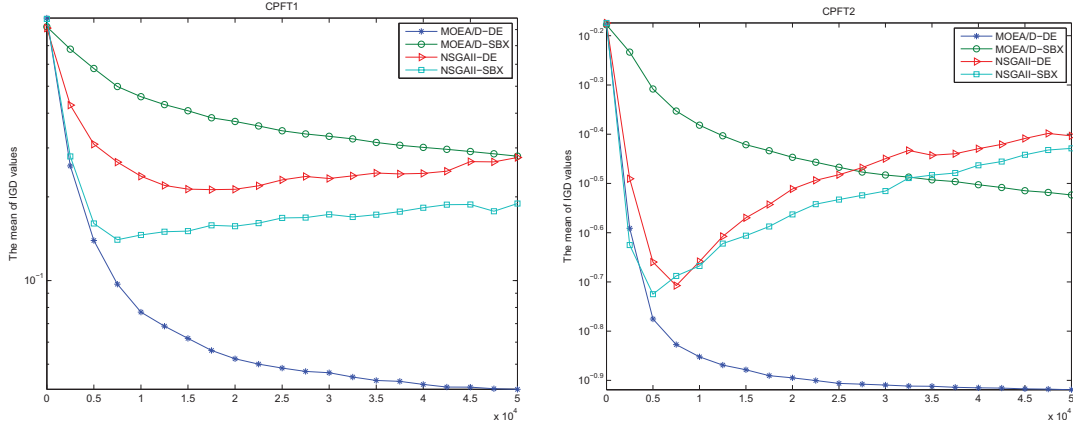


Fig. 12. Convergence of MOEA/D and NSGA-II in terms of IGD values over the number of function evaluations on CPFT1 (left) and CPFT2 (right)

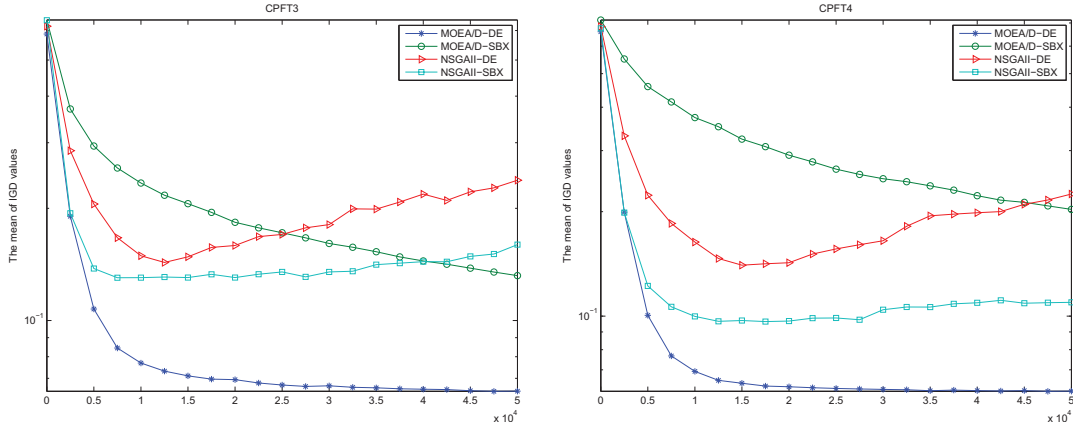


Fig. 13. Convergence of MOEA/D and NSGA-II in terms of IGD values over the number of function evaluations on CPFT3 (left) and CPFT4 (right)

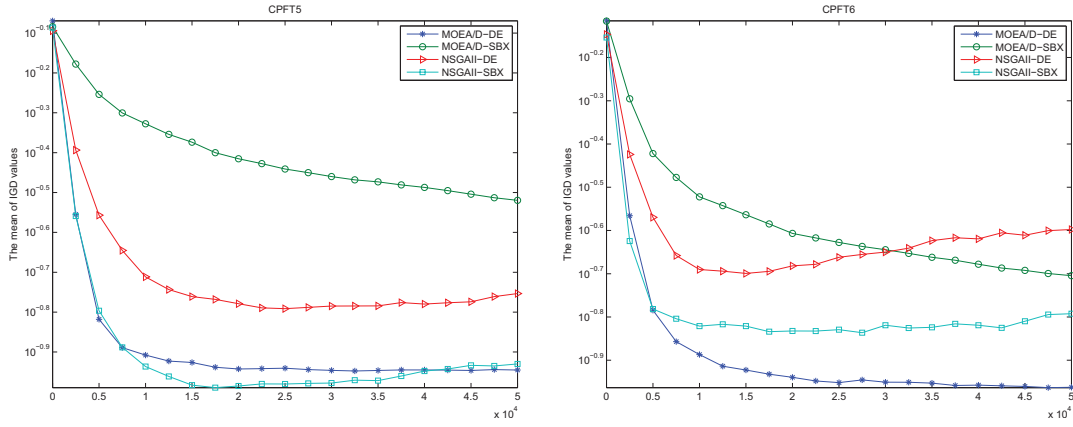


Fig. 14. Convergence of MOEA/D and NSGA-II in terms of IGD values over the number of function evaluations on CPFT5 (left) and CPFT6 (right)

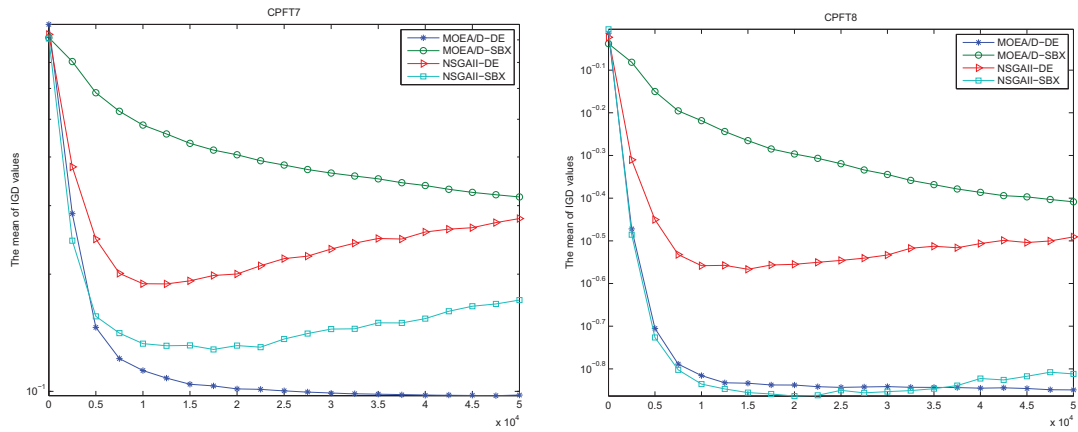


Fig. 15. Convergence of MOEA/D and NSGA-II in terms of IGD values over the number of function evaluations on CPFT7 (left) and CPFT8 (right)

NSGA-II can get worse as the search proceeds. The reason is that the crowding distance for density estimation in NSGA-II is not very effective for the MOPs with more than two objectives. In the case of 3 objectives, more nondominated solutions near the boundary of 2-D Pareto fronts are preferred in selection.

Figs. 16-18 plot the final solutions with the minimal IGD values in 20 runs found by MOEA/D-DE and NSGA-II/SBX on CPFT1-CPFT3, which correspond to 1-D, 2-D, and mixed dimensionality in the POFs. It is evident that MOEA/D-DE is superior to NSGA-II/SBX in convergence. NSGA-II/SBX fails to find the solutions in the centering part of POFs. For other instances, the situations are quite similar.

From the above results, we can see that both MOEA/D and NSGA-II have weaknesses in diversifying POFs during the multiobjective search. The decomposition of MOPs in MOEA/D may not be able to produce suitable weight vectors for subproblems when the POFs are degenerated. If a set of uniform weight vectors are used in MOEA/D, the optimal solutions of subproblems are not evenly distributed. Therefore, adaptive weighting strategy should be a good option in MOEA/D for the MOPs with complicated Pareto fronts.

## V. CONCLUSIONS

The degeneracy of Pareto fronts is a difficult feature for many MOEAs. This paper mainly focuses on how to generate multiobjective test instances with various degenerate Pareto fronts. To verify the difficulties of these test instances, we also conducted some experiments to study the behaviors of two popular MOEAs, i.e., MOEA/D and NSGA-II. From the experimental results presented in this paper, the test instances with degenerated Pareto fronts can not be solved well both in convergence and in diversity. To have better performance, more efficient strategies should be used in MOEA/D and NSGA-II. For example, adaptive weighting method is very important in MOEA/D for these instances. This is also our future research work.

## ACKNOWLEDGMENT

The authors would like to thank the anonymous reviewers for their insightful comments. This work was supported by National Natural Science Foundation of China (NSFC) grants 61175063 and 11131006.

## REFERENCES

- [1] A. Zhou, B.Y. Qu, H. Li, S.Z. Zhao, P.N. Suganthan, and Q. Zhang. Multiobjective Evolutionary Algorithms: A Survey of the State of the Art. *Swarm and Evolutionary Computation*, 1(1):32–49, 2011.
- [2] K. Deb. Multi-objective Genetic Algorithms: Problem Difficulties and Construction of Test Problems. *Evol. Comput.*, 7(3):205–230, 1999.
- [3] S. Huband, P. Hingston, L. Barone, and L. While. A Review of Multiobjective Test Problems and a Scalable Test Problem Toolkit. *IEEE Trans. on Evolutionary Computation*, 10(5):477–506, 2006.
- [4] H. Li and Q. Zhang. A Multiobjective Differential Evolution Based on Decomposition for Multiobjective Optimization with Variable Linkages. In *PPSN*, pages 583–592, 2006.
- [5] Q. Zhang, A.M. Zhou, and Y.C. Jin. RM-MEDA: A Regularity Model-Based Multiobjective Estimation of Distribution Algorithm. *IEEE Trans. Evolutionary Computation*, 12(1):41–63, 2008.
- [6] H. Li and Q. Zhang. Multiobjective Optimization Problems with Complicated Pareto Sets, MOEA/D and NSGA-II. *IEEE Trans. on Evolutionary Computation*, 2(12):284–302, 2009.
- [7] Q. Zhang, A.M. Zhou, S.Z. Zhao, P. N. Suganthan, W.D. Liu, and S. Tiwari. Multiobjective optimization Test Instances for the CEC 2009 Special Session and Competition. Technical report, CES-887, School of Computer Science and Electrical Engineering, University of Essex, 2008.
- [8] K. Miettinen. *Nonlinear Multiobjective Optimization*. Kluwer International Series in Operations Research & Management Science. Kluwer, Norwell, MA, 1999.
- [9] E. Zitzler, M. Laumanns, and L. Thiele. SPEA2: Improving the Strength Pareto Evolutionary Algorithm for Multiobjective Optimization. In K. C. Giannakoglou, D. T. Tsahalis, J. Périaux, K. D. Papailiou, and T. Fogarty, editors, *Evolutionary Methods for Design Optimization and Control with Applications to Industrial Problems*, pages 95–100, Athens, Greece, 2001.
- [10] K. Deb, S. Agrawal, A. Pratap, and T. Meyarivan. A fast and elitist multiobjective genetic algorithm: NSGA-II. *IEEE Trans. Evolutionary Computation*, 6(2):182–197, 2002.
- [11] Q. Zhang and H. Li. MOEA/D: A Multiobjective Evolutionary Algorithm Based on Decomposition. *IEEE Trans. Evolutionary Computation*, 11(6):712–731, 2007.
- [12] Eckart Zitzler and Simon Knzli. Indicator-based selection in multiobjective search. In *Proc. 8th International Conference on Parallel Problem Solving from Nature (PPSN VIII)*, pages 832–842. Springer, 2004.
- [13] E. Zitzler, K. Deb, and L. Thiele. Comparison of Multiobjective Evolutionary Algorithms: Empirical Results. *Evol. Comput.*, 8(2):173–195, 2000.
- [14] K. Deb, L. Thiele, M. Laumanns, and E. Zitzler. Scalable Test Problems for Evolutionary Multi-Objective Optimization. Technical report, Kanpur Genetic Algorithms Lab. (KanGAL), Indian Inst. Technol., Kanpur, India, 2001. KanGAL Report 2001 001.

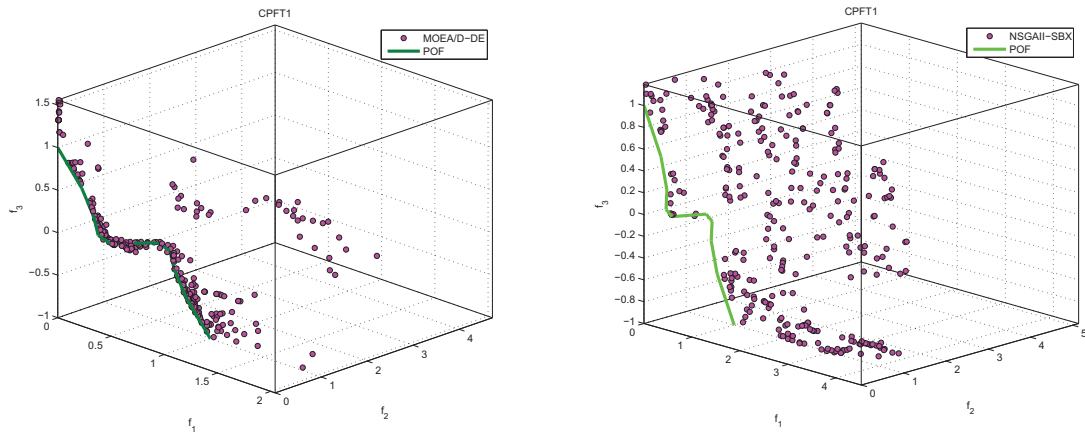


Fig. 16. Plots of final populations of MOEA/D and NSGA-II in the best run on CPFT1

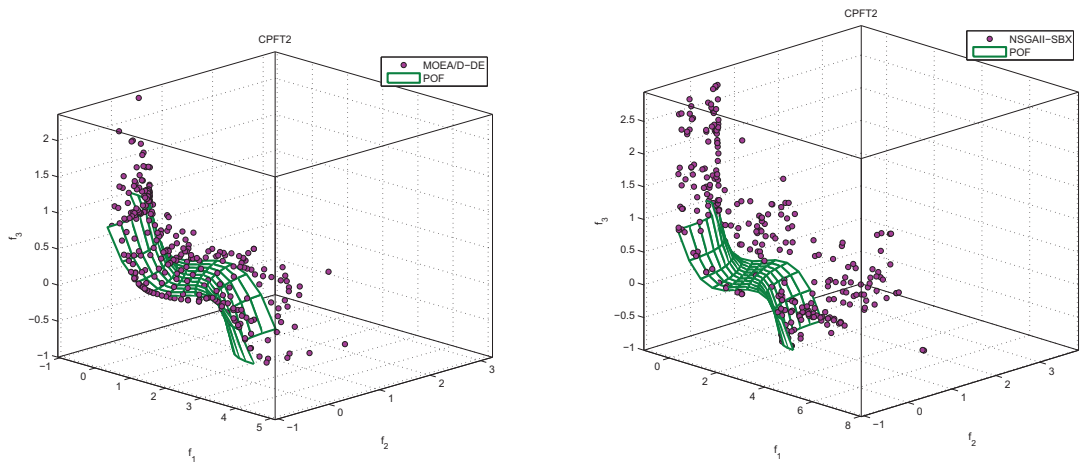


Fig. 17. Plots of final populations of MOEA/D and NSGA-II in the best run on CPFT2

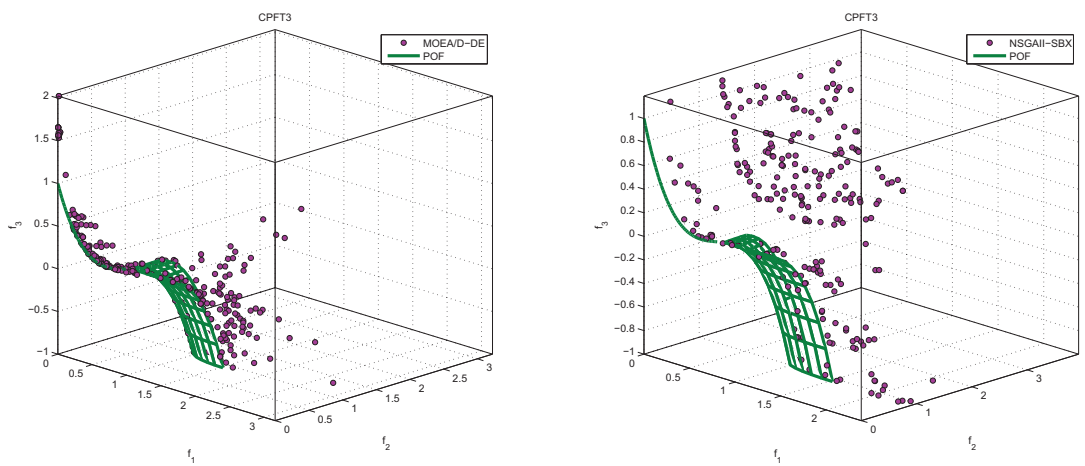


Fig. 18. Plots of final populations of MOEA/D and NSGA-II in the best run on CPFT3